Sensors and Actuators A, 29 (1991) 185–193

An integrated miniature capacitive pressure sensor

Takeshi Kudoh*, Shuichi Shoji and **Masayoshi Esashi**

Department of Mechatronics and Precision Engineering, Tohoku University, Aza Aoba, Aramaki Aoba-ku, Sendai 980 (Japan)

(Received May 16, 1991; accepted July 22, 1991)

Abstract

A newly designed capacitive pressure sensor which incorporates a CMOS IC on the same silicon chip has been developed. The sensor chip is 3.3 mm×3.7 mm×0.5 mm in size, and both the sensing capacitive element and the electronic circuit are hermetically sealed between the silicon substrate and the glass cover using a unique electrical feedthrough structure. The incorporated electronic circuit is the *C–F* converter whose oscillation frequency changes as a function of the sensing capacitance. By optimizing the circuit supply voltage, the thermally induced baseline (oscillation frequency at atmospheric pressure) drift can be reduced to within 3.1% F.S. between 20 °C and 50 °C. Since the oscillation frequency can be counted by the consumed current pulses, the pressure waveform can be monitored with only two external leads.

1. Introduction

High-performance miniature pressure sensors are in great demand for many fields, such as medical instrumentation, automobile engine control as well as industrial purposes. These sensors must have sufficient sensitivity, good stability, high signal-to-noise ratio, etc. Among the many pressure-sensing instruments in use, piezoresistive sensors are widely used owing to their simple structure and ease of manufacture. Continuing investigations [1–4] have enabled well-developed products to become commercially available. However, piezoresistive sensors have the following disadvantages:

(1) limited pressure sensitivity, which comes from the piezoresistive coefficient of silicon;

(2) weakness to the stress which is induced in the packaging process;

(3) thermally induced baseline drift caused by the relatively large temperature coefficient of the piezoresistive element.

Consequently, individual sensor chips need adjustments to obtain good accuracy.

Capacitive sensors, on the other hand, employ a parallel-plate capacitor formed between a fixed electrode and a silicon diaphragm as the pressure-sensing element. Since the silicon diaphragm is thin enough to be bent by the applied pressure, the displacement of the diaphragm leads to a capacitance increase. In contrast to the piezoresistive sensors which utilize a small change (less than a few percent) of resistance caused by the applied pressure, capacitive sensors have high sensitivity due to the relatively large capacitance change (a few tens percent [5, 6]). Therefore capacitive sensors are scarcely affected by packaging stress, etc., and have better stability than the conventional piezoresistive sensors.

Capacitive sensors, however, need electronic circuits to convert the capacitance to electrical signals with low output impedance. For the 'miniature' capacitive sensor, the electronic circuit should be placed close to the sensing capacitor to reduce the stray capacitance which may obscure the actual pressure signals. Such sensors have been investigated in the last two decades by combining silicon micromachining and integrated circuit technology.

In accordance with the fabrication process, capacitive sensors with an electronic circuit are divided into two types as follows. One

*Present address: Tech. R&D Center, Terumo Corporation, 1500 Inokuchi, Nakai-cho, Ashigarakami-gun, Kanagawa 259-01, Japan.

0924-4247/91/$3.50

type is the hybrid sensor [6–11], whose sensing chip and electronic circuit chip are fabricated separately and assembled. Optimized processes can be used for both sensor and circuit chips. The other type is the monolithic or integrated sensor, which has a sensing element and an electronic circuit on the same silicon chip [5, 12, 13]. This method has some advantages in reduction of stray capacitance and in miniaturization of the sensor.

In spite of these investigations, miniature capacitive sensors have not yet been practically used because of some difficulties, for example, encapsulation. This paper describes the outline, the fabrication process and the performance of an integrated miniature capacitive pressure sensor with a novel electrical feedthrough structure.

2. The outline of the sensor

2.1. Structure

The structure of the fabricated pressure sensor is illustrated in Fig. 1. The sensor chip is 3.7 mm×3.3 mm×0.5 mm in size and consists of anodically bonded glass and silicon chips. A hermetically sealed reference cavity is formed between them. Two integrated circuits and a pressure-sensing diaphragm which acts as the movable electrode of the pressure-sensing capacitor are fabricated on the same silicon substrate. On the other hand, the glass surface has the evaporated aluminium electrode of the capacitor. The portion over the electronic circuits is also covered with aluminium, which acts as a light shield to prevent the photovoltaic effect. One of the two integrated circuits enclosed in the reference cavity is selected for use in the metallizing process. An interconnection between the circuit and the fixed electrode is obtained by bringing a metallized boss on the silicon substrate into contact with an aluminium lead of the fixed electrode. Three external leads are attached with conductive epoxy to metallized contact-pads inside small glass holes. Although this sensor requires only one pair of power-supplying leads for pressure detection, the other lead can be used just for monitoring the output voltage waveform. Electrical feedthrough from the circuit is taken to the outside without breaking the hermetic seal by means of the novel feedthrough structure described later.

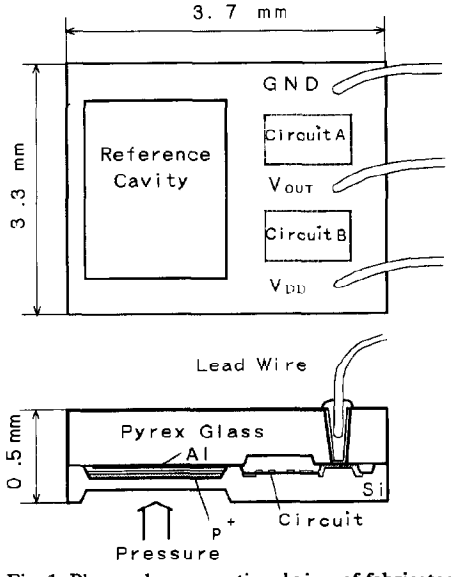

Fig. 1. Plan and cross-sectional view of fabricated pressure sensor.

Applying pressure P (mmHg) to a rectangular silicon diaphragm with a centre boss, the displacement of the centre of the diaphragm $w(P)$ (μm) is given by [14, 15]

$$w(P) = 1.56\times10^{-11}\frac{(2a)^4}{h^3}(1-\alpha)^2P \qquad (1)$$

$$= KP$$

where $2a$ (μm) is a dimension of the diaphragm, h (μm) the thickness of the diaphragm and α is b/a ($2b$ is the dimension of the mesa). The proportionality coefficient K is the constant value determined by these parameters. Equation (1) shows that $w(P)$ increases in proportion to P. It should be noted that $w(P)$ is also proportional to h^{-3}, so thickness control of the diaphragm is very critical for achieving the designed performance. Since the circuit is designed so that the oscillation frequency $f(P)$ is proportional to $1/C_x$, $f(P)$ is given by a linear function of P as

$$f(P) = f_0\frac{C_0}{C_x} = f_0\frac{d-KP}{d}$$

$$= f_0\left(1-\frac{K}{d}P\right) \qquad (2)$$

where f_0 is the zero-pressure frequency, C_0 is the zero-pressure capacitance of C_x and d is the capacitor's gap. Equation (2) shows that the frequency decreases linearly by a factor $-K/d$ as the pressure increases. In order to obtain a high sensitivity and to reduce the influence of stray capacitance, the capacitor's gap has to be as narrow as possible. Consequently the gap was designed to be 1 μm considering the fabrication feasibility. The maximum displacement of the diaphragm, w_{max}, is limited to within 0.5 μm because the passivation film (PSG/SiO_2) of thickness 0.5 μm is on the movable electrode. Substituting the pressure P (300 mmHg), w_{max} (0.5 μm), α (0.6) and the dimension of the diaphragm $2a$ (2000 μm) into eqn. (1) yields a diaphragm thickness of 30 μm.

2.2. *Capacitance to frequency converter*

This sensor includes two CMOS integrated circuits as illustrated in Fig. 2 for capacitance to frequency (C–F) conversion. Figure 2(a) shows the one using a Schmitt-trigger circuit. The oscillation frequency depends on the capacitance C_x, its charging current I_C and on the discharging current I_D. Another C–F converter using an astable multivibrator is shown in Fig. 2(b). The charging and discharging currents flow through MOS transistors P1 and N1 respectively. The oscillation frequency can be detected by monitoring the currents that flow just at the moment of inversion.

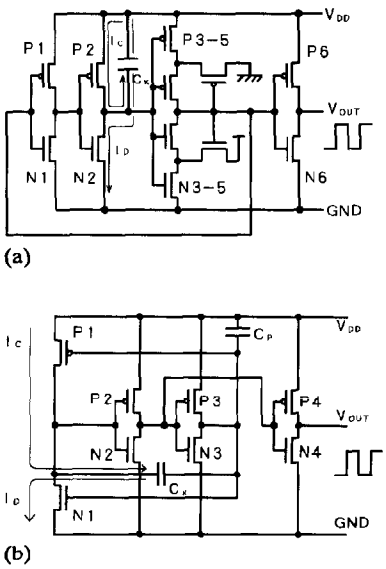

Fig. 2. Capacitance to oscillation frequency converter circuits using (a) Schmitt trigger and (b) astable multivibrator, respectively.

For practical use of the sensor, thermal drift of the oscillation frequency becomes a problem. The drift in the circuit is caused mainly by the thermally induced variation of the charging and discharging currents. Therefore the oscillation circuits were designed so as to have a current-regulation mechanism to the temperature change explained as follows. The drain current I_d of a MOS transistor at the temperature T is given by

$$I_d = \frac{W}{2L}\mu(T)C_{OX}(V_{GS}-V_{th}(T))^2 \tag{3}$$

where W is the channel width, L the channel length, C_{OX} the gate capacitance for unit area, V_{GS} the voltage between the gate and source, $\mu(T)$ the carrier mobility and $V_{th}(T)$ the threshold voltage. By differentiating eqn. (3) with respect to T, the thermally induced variation of the drain current, dI_d/dT, is found as

$$\frac{dI_d}{dT} = \frac{WC_{OX}}{2L} \times\left[\frac{d\mu}{dT}(V_{GS}-V_{th})^2-2\mu(V_{GS}-V_{th})\frac{dV_{th}}{dT}\right] \tag{4}$$

Both $d\mu/dT$ and dV_{th}/dT are negative in MOS transistors, therefore, the first term of eqn. (4) is negative and the second is positive. The temperature compensation for drain current can thus be realized at an appropriate voltage V_{GS} by counter balancing the two terms. Since V_{GS} is controllable by varying the supply voltage V_{DD} in these circuits, the thermally induced baseline drift can be compensated by providing an appropriate V_{DD}.

3. Fabrication process

The fabrication process of the sensor is shown in Fig. 3. A silicon substrate (Fig. 3(a), (b)) and a glass cover (Fig. 3(c), (d)) were processed separately and were then bonded anodically (Fig. 3(e)). After the bonding process, the sensing diaphragm was formed (Fig.

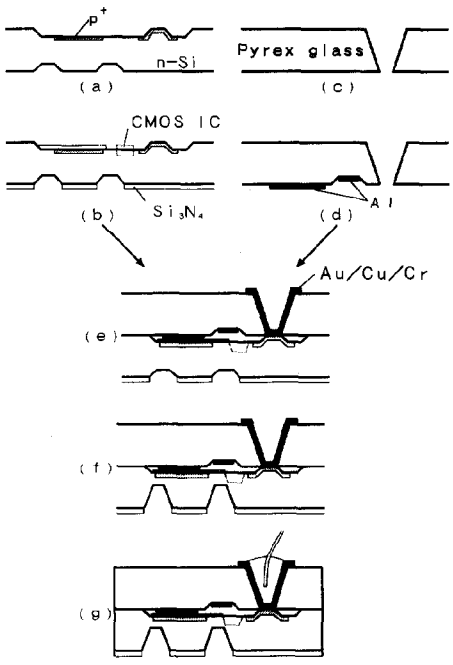

Fig. 3. Schematic diagram of sensor fabrication process.

3(f)) and external leads were then attached (Fig. 3(g)).

3.1. Silicon substrate

The starting material is a low-doped (resistivity 4–8 Ω cm) n-type single-crystalline (100) silicon substrate 20 mm × 20 mm in size with a thickness of 0.2 mm. Twenty sensor chips were batch fabricated on it. The fabrication was started by forming the capacitor's gap. The silicon surface facing the reference cavity was partly etched by 2 μm using 35. wt.% KOH solution at 80 °C with an SiO_2 mask. At the same time, a sensing diaphragm was patterned on the back side using a double-sided alignment technique. Boron was then diffused for the p^+ capacitor diffusion electrode and for the contact-pads as well as for the guard-ring of the CMOS p-well. The CMOS IC was fabricated with the polysilicon gate 10 μm rule technology [16]. It should be noticed that a sensing capacitor and CMOS IC could be fabricated all on one chip through successive processes. Microphotographs of the *C–F* converter circuits using a Schmitt trigger and astable multivibrator are shown in Fig. 4(a) and (b) respectively.

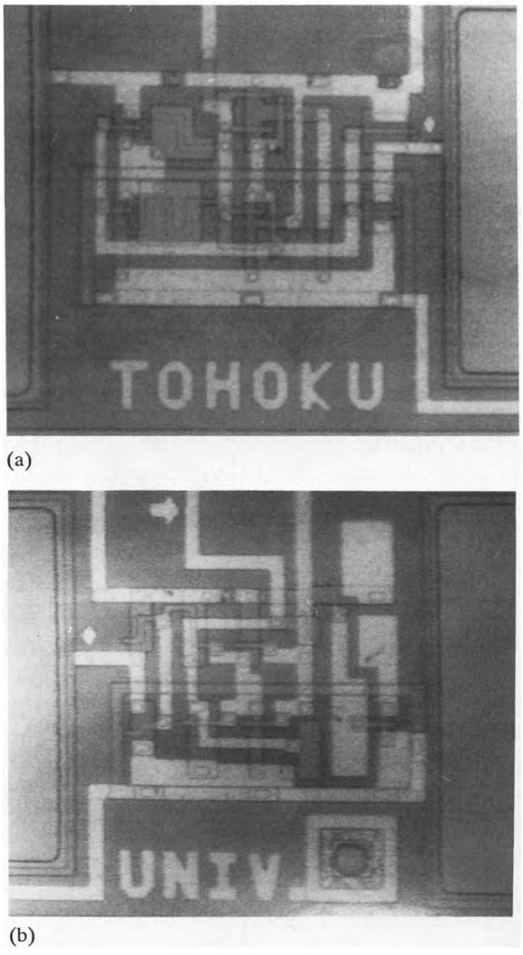

Fig. 4. Microphotographs of the integrated C–F converter circuits using (a) Schmitt trigger and (b) astable multivibrator respectively.

3.2. Glass cover and construction

The glass cover is Pyrex glass 20 mm × 20 mm in size with a thickness of 0.3 mm. Sixty small through-holes for external-lead bonding were bored using electrochemical discharge drilling [17]. A high aspect ratio of 300 μm in thickness and 120 μm in bottom diameter was obtained. The glass cover over the electronic circuits was then partly etched out with concentrated hydrofluoric acid using a gold/chromium mask. Following the gold/chromium mask removal, aluminium is evaporated and patterned as the fixed electrode, the metallized leads and the light shield of the electronic circuits.

The silicon and the glass were bonded anodically. Since this sensor includes a C–F

converter circuit in the reference cavity, electrical feedthrough without any leakage is needed. Figure 5 shows the novel hermetically sealed electrical feedthrough structure. As is shown in Fig. 5, p^+ diffused silicon acts as the electrical conductor and the hermetic seal is achieved by anodic bonding around the through-holes of the glass cover. The validity of anodic bonding for the hermetic seal has been proved in the packaging scheme of conventional piezoresistive sensors [17]. Since no steps appear in the silicon surface with this structure, an air-leakage channel is not formed. Furthermore, current-leakage problems due to unpassivated p–n junctions do not occur because all the p–n junctions are oxide passivated and are not bonded to the glass cover.

In the anodic bonding process, both silicon and the glass cover were heated up to 400 °C and a high voltage (600–1000 V) was applied between them. In spite of not being shielded from the high voltage, the integrated

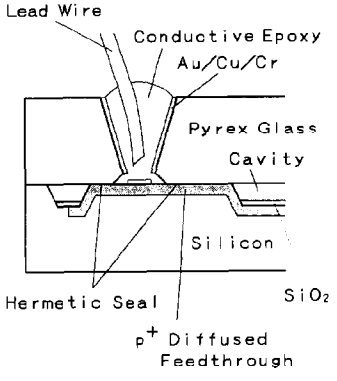

Fig. 5. Newly designed hermetically sealed electrical feedthrough structure.

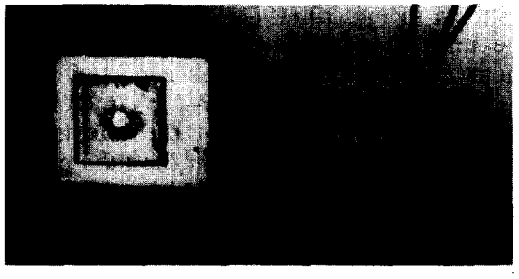

(a) (b)

Fig. 6. Photographs of the completed sensor chip. (a) Silicon diaphragm side view. (b) Glass cover side view with three external leads.

circuits were not damaged at all. We believe this is because the high voltage was not applied to the gate oxide, since the polysilicon gate and the silicon substrate were at the same potential due to the interconnection between the gate and the substrate (i.e., source and drain of the MOS transistor). The pressure in the reference cavity was 1 atm at the bonding temperature, therefore the inner pressure becomes about 0.4 atm at room temperature. The anodic bonding can also be performed in compressed air (e.g., 2.5 atm) or in vacuum. The former will give a reference cavity at 1 atm and the latter an evacuated one.

Following the anodic bonding process, a conducting layer of Au/Cu/Cr was evaporated on the inside of the small glass holes through the molybdenum metal mask for lead attachment (see Fig. 5). The sensing diaphragm was then formed by etching with KOH solution at 75 °C until the designed thickness was obtained. The glass cover side needs to be protected with wax throughout the etching process. It should be noted that small packaged sensors have been fabricated through a successive batch process. The etched substrate is diced into each chip. Three external leads (polyurethane-coated Cu wire of 100 μm diameter) are connected to the chip with conductive epoxy. Tin solder is also available for the lead connection. Mechanically sturdy attachment of a lead wire is achieved by putting it into a glass hole. Figure 6 shows photographs of a completed sensor chip. A silicon diaphragm side view and a glass cover side view with three external leads are seen in Fig. 6(a) and (b) respectively.

4. Performance

4.1. Experimental

Figure 7 shows a block diagram of the measuring system. The sensor was placed in a pressure chamber with a thermocontroller. Pressure was fed into the chamber from a pressure controller. A regulated voltage was supplied to the sensor. A current mirror IC (TL014C) was connected between the voltage supply and the sensor so that the consumed current could be detected as a voltage drop across the load resistance R_L. The resulting

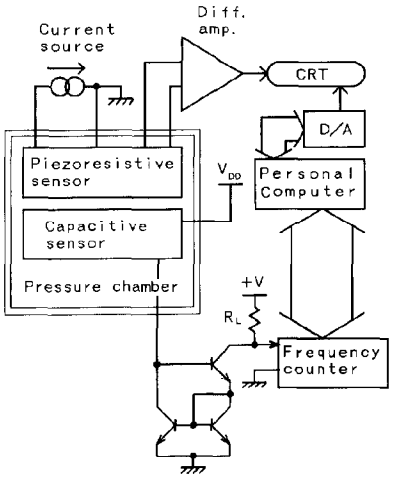

Fig. 7. Block diagram of the measuring system.

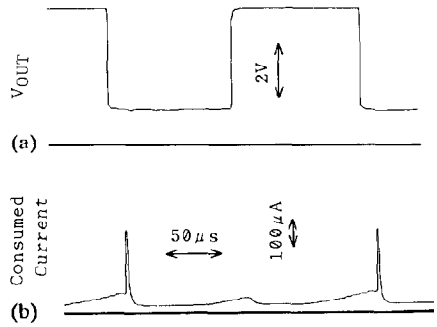

Fig. 8. Dissipated current pulses (b) in conjunction with the output voltage waveforms (a).

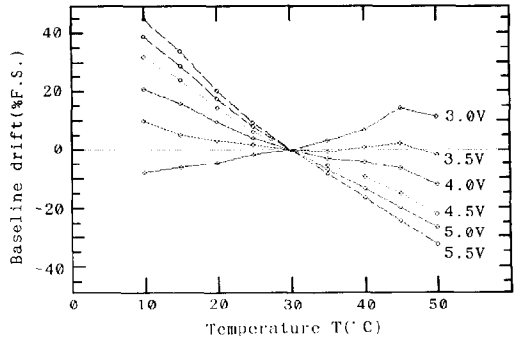

Fig. 9. Thermally induced baseline drifts for each supply voltage.

voltage waveform was fed into a signal-conditioning circuit and the oscillation frequency was detected by a counter. The resultant value was accumulated by a personal computer for data processing. A pressure-corresponding analog voltage was also available from the computer through a D/A converter for an oscilloscope. A commercial piezoresistive sensor was used just for the pressure waveform monitoring. Both output voltages of the piezoresistive sensor and of the D/A converter were observed and recorded simultaneously using an oscilloscope.

4.2. Results

In order to clarify and to simplify the description, the experimental results from the sensor with the Schmitt-trigger circuit are shown here, though the other circuit also worked.

Figure 8 shows the consumed current pulses (b) in conjunction with the output voltage waveforms (a) at a pressure of 760 mmHg. The current pulses appear at the moment when the output voltage decreases. Figure 8 is an example recorded at $V_{DD}=3.5$ V, which shows that the consumed electric power is about 40 μW. This value is almost two orders of magnitude less than that of conventional piezoresistive sensors.

Figure 9 shows the thermally induced baseline (oscillation frequency at atmospheric pressure) drifts for each supply voltage between 3.0 V and 5.5 V. Each baseline drift is represented in comparison with the value at 30 °C. It should be noticed that the baseline drift is compensated at an appropriate supply voltage (3.5 V), as discussed in Section 2.2. At $V_{DD}=3.5$ V, the drift is reduced to within 3.1% of full scale (%F.S.) in the temperature range between 20 °C and 50 °C.

The oscillation frequency response as a function of applied pressure (i.e., *P–F* characteristic with temperature as a parameter) is shown in Fig. 10 ($V_{DD}=3.5$ V). A straight line in Fig. 10 represents the slope of the linear *P–F* characteristic. As expected from eqn. (2), an almost linear *P–F* characteristic was obtained. The slope of the line is the averaged value deduced from the data points between 758 mmHg and 1028 mmHg at 20 °C. The pressure sensitivity found by the slope was 0.35 mmHg/Hz at 760 mmHg. Although the baseline drift was compensated for the temperature change at 760 mmHg, an uncompensated sensitivity change with temperature resulted. The non-linearity of the *P–F*

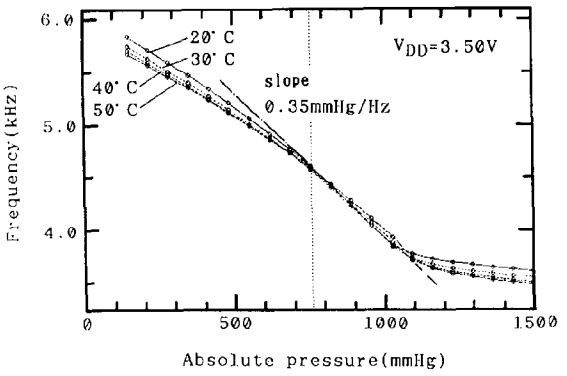

Fig. 10. Oscillation frequency response as a function of applied pressure (*P–F* characteristic).

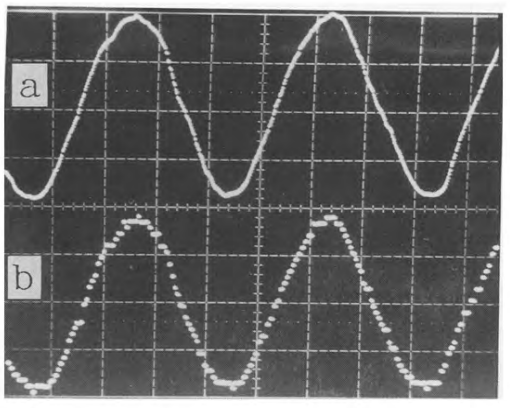

Fig. 11. Oscillograms of monitored pressure waveforms using (a) piezoresistive sensor and (b) capacitive sensor respectively. *x*-axis: time (0.5 s/div). *y*-axis: pressure (50 mmHg/div).

characteristic shows that the sensitivity changes with the applied pressure. Furthermore, it may also suggest the existence of a stray capacitance connected parallel to the real sensing capacitor. When the pressure exceeds about 1000 mmHg, the slope of the *P–F* characteristic decreases. This change of slope infers that the diaphragm is being touched by the fixed electrode. Owing to this limited displacement, the diaphragm was not broken even when excess pressure was applied. The gradual frequency drop with increased excess pressure is supposed to be a result of the increase in touching area.

Figure 11 shows the monitored pressure waveforms using (a) a piezoresistive sensor and (b) a capacitive sensor, respectively. The waveform in Fig. 11(b) agrees well with that in Fig. 11(a). These values were recorded within the pressure range where the capacitive sensor had nearly linear *P–F* characteristics. The voltage supplied to the capacitive sensor was 5.0 V so as to obtain higher sensitivity and the ambient temperature was kept at 20 °C throughout the measurement. Since a detectable pressure difference is deduced from the product of the sampling frequency and the pressure change corresponds to unit frequency, the pressure resolution (i.e., the ratio of detectable pressure difference to full-scale pressure), *Res*, is expressed as

$$Res = 100SF/H \text{ (\% of full scale)} \quad (5)$$

where S is the pressure change per unit frequency (0.12 mmHg/Hz), F is the sampling frequency (50 Hz) and H is the full-scale pressure (200 mmHg). The substitution of the values in parentheses, which are those applied in this experiment, yields a resolution of 3% F.S.

5. Discussion

In order to obtain a large base capacitance, the capacitor's gap should be designed to be as narrow as possible. After determining the gap, the diaphragm thickness h, which relates to K in eqn. (2), is calculated so as to obtain the required full-scale pressure.

In this fabrication process, the signal-processing circuits were fabricated on the etched surface. These circuits, however, could be fabricated on a bare silicon surface by etching only the capacitor diffusion area.

The pressure-dependent sensitivity (i.e., non-linearity) may be caused in part by the stray capacitance and the non-ideal parallel-plate capacitor of the pressure-sensing element. Assuming that the diaphragm moves perpendicular to the fixed electrode and further that there was no stray capacitance, the sensor sensitivity can be expressed as eqn. (2). The diaphragm, however, is not kept parallel to the fixed electrode by diaphragm bending. In order to keep the two electrodes as parallel as possible, the diaphragm area should be covered with a boss, i.e., a central hard plate.

On the other hand, the thermally-induced variation of the sensor output is assumed to come from: (1) the expansion of the air in

the reference cavity; (2) the variations of charging and discharging currents in the circuit; and (3) thermally induced stress, which comes from the different thermal expansion coefficients of silicon and Pyrex glass.

In the case of anisotropic etching of (100) silicon, oblique (111) planes appear at the surrounding rims of the diaphragm during the etching progress. The oblique planes occupy a relatively large area. If the edge of the diaphragm could be etched perpendicularly, the completed sensor would be smaller. Ion-etching is expected to achieve such perpendicular etching. Another method to realize the small sensor is to use the rim-less structure diaphragm [10, 13].

Controlling the diaphragm thickness is very important for obtaining the designed sensitivity. Since the sensitivity is proportional to h^{-3}, as described in eqns. (1) and (2), precise diaphragm thickness control is needed. Etching control methods such as electrochemical etch-stop [18] or doping-selective etching [19] are expected to give uniform performance of the sensors.

As mentioned in Section 3.2, this sensor has a low-pressure (about 0.4 atm) reference cavity. In the case of an evacuated reference cavity, the atmospheric pressure causes an offset diaphragm displacement which causes difficulty in precise low-pressure measurement. On the other hand, the sensor with atmospheric cavity pressure is expected to have a high pressure resolution, but thermal air expansion in the reference cavity will cause thermal drift. This intrinsic property of an absolute pressure sensor requires proper design according to the purpose required.

This sensor can compensate the thermally induced baseline drift by supplying an appropriate voltage; however, the temperature range compensated within 3% F.S. is limited between 20 °C and 50 °C. Moreover the sensitivity is not compensated properly. In order to extend the compensated temperature range and to compensate the sensitivity, appropriate compensation circuits are needed.

The pressure-detection system in this experiment shown in Fig. 7 is based on frequency counting. Although this method can utilize the linear relation between applied pressure and oscillation frequency, a long detection period is needed in principle to obtain a high resolution. As a result, sampling cut-off frequency is traded for pressure resolution. On the other hand, a precise (high-speed clock) period counter which detects the pressure during one or several time periods will drastically improve both the pressure resolution and the sampling cut-off frequency [13]. If a period counter is used, a numerical data processor which converts the resulting period to the equivalent frequency is needed to utilize the linear pressure–frequency characteristic.

6. Conclusions

An integrated miniature capacitive pressure sensor has been fabricated by a newly designed process. A CMOS IC, electrical feedthrough and a pressure-sensing diaphragm have been fabricated. A batch-process encapsulation was developed with the newly designed sealed structure.

The fundamental performance of the sensor has been evaluated and the sensor has demonstrated the monitoring of a pressure waveform with only two external leads.

Some suggestions toward the design and the fabrication of improved sensors have been presented. Although small packaged integrated sensors have not been manufactured yet, it is expected that the fabrication process developed here will be applied for many kinds of small-size integrated sensors with high performance and low cost.

Acknowledgements

The authors wish to acknowledge helpful discussions with Mr Matsumoto of Tohoku University. This work was supported in part by a Grant-in-aid for Scientific Research from the Ministry of Education, Science, and Culture (63850084).

References

1 J. M. Borkey and K. D. Wise, Integrated signal conditioning for silicon pressure sensors, *IEEE Trans. Electron Devices, ED-26* (1979) 1906–1910.

2 M. Esashi, H. Komatsu, T. Matsuo, M. Takahasi, T. Takashima, K. Imabayashi and H. Ozawa, Fabrication of catheter-tip and sidewall miniature pressure sensors, *IEEE Trans. Electron devices, ED-29* (1982) 57–63.

3 S. Sugiyama, M. Takigawa and I. Igarashi, Integrated piezoresistive pressure sensor with both voltage and frequency output, *Sensors and Actuators, 4* (1983) 113–120.
4 I. Igarashi, Semiconductor dynamic sensors, *Sensors and Actuators, 13* (1988) 53–62.
5 C. S. Sander, J. W. Knutti and J. D. Meindl, A monolithic capacitive pressure sensor with pulse-period output, *IEEE Trans. Electron Devices, ED-27* (1980) 927–930.
6 H. L. Chau and K. D. Wise, An ultraminiature solid-state pressure sensor for a cardiovascular cathether, *IEEE Trans. Electron Devices, 35* (1988) 2355–2362.
7 J. T. Suminto, G. J. Yeh, T. M. Spear and W. H. Ko, Silicon diaphragm capacitive sensor for pressure, flow, acceleration and attitude measurements, *Proc. 4th Int. Conf. Solid-State Sensors and Actuators (Transducers '87), Tokyo, Japan, June 2–5, 1987,* pp. 336–339.
8 W. H. Ko, Solid-state capacitive pressure transducers, *Sensors and Actuators, 10* (1986) 303–320.
9 A. Hanneborg, T. E. Hansen, P. A. Ohlckers, E. Carlson, B. Dahl and O. Holwech, An integrated capacitive pressure sensor with frequency-modulated output, *Sensors and actuators, 9* (1986) 345–351.
10 K. Furuta, M. Esashi, S. Shoji and Y. Matsumoto, Catheter-tip capacitive pressure sensor, *Tech. Digest, 8th Sensor Symp. Japan, 1989,* p. 25–28.
11 W. H. Ko, M. H. Bao and Y. D. Hong, A high-sensitivity integrated-circuit capacitive pressure transducer, *IEEE Trans. Electron Devices, ED-29* (1982) 48–56.
12 W. H. Ko, B. X. Shao, C. D. Fung, W. J. Shen and G. J. Yeh, Capacitive pressure transducers with integrated circuits, *Sensors and Actuators, 4* (1983) 403–411.
13 Y. Matsumoto, S. Shoji and M. Esashi, A miniature capacitive pressure sensor, *Tech. Digest, 9th Sensor Symp. Japan, 1990,* pp. 43–46.
14 B. Puers, E. Peeters and W. Sansen, CAD tools in mechanical sensor design, *Sensors and Actuators, 17* (1989) 423–429.
15 Y. S. Lee and K. D. Wise, A batch-fabricated silicon capacitive pressure transducer with low temperature sensitivity, *IEEE Trans. Electron. Devices, ED-29* (1982) 42–48.
16 H. Seo, M. Esashi and T. Matsuo, Fabrication of CMOS LSI for implantable biotelemeter, *IEICE Tech. Rep., 1986,* pp. 15–22.
17 M. Esashi, Y. Matsumoto and S. Shoji, Absolute pressure sensors by air-tight electrical feedthrough structure, *Sensors and Actuators, A21–A23* (1990) 1048–1052.
18 B. Kloeck, S. D. Collins, N. F. de Rooij and R. L. Smith, Study of electrochemical etch-stop for high-precision thickness control of silicon membranes, *IEEE Trans. Electron Devices, ED-36* (1989) 663–669.
19 Y. Linden, L. Tenerz, J. Tiren and B. Hoek, Fabrication of three-dimensional silicon structures by means of doping-selective etching (DSE), *Sensors and Actuators, 16* (1989) 67–82.

Biographies

Takeshi Kudoh received the B.E. degree in applied physics and M.C. Degree in engineering from Tohoku University, Sendai, Japan, in 1985 and 1987 respectively.

In 1987, he joined the Terumo Corporation, Japan. From 1987 to 1990, he was at Tohoku University, where he was engaged in the research and development of the integrated capacitive pressure sensor. Since 1989 he has been with the Tech. R&D Center, Terumo Corporation. Most recently his interest has centred on the development of physical sensors for biomedical applications.

Shuichi Shoji received the B.E. degree in electronic engineering and the Ph.D. degree in engineering from Tohoku University in 1979 and 1984 respectively.

From 1984 to 1990, he was a research associate of the Electronic Engineering Department of Tohoku University. He is now a research associate of the Mechatronics and Precision Engineering Department of Tohoku University. His current research is on micro flow devices and micromechanical devices fabricated by micromachining.

Masayoshi Esashi received the B.E. degree in electronic engineering and the Ph.D. degree in engineering from Tohoku University, Japan, in 1971 and 1976 respectively.

From 1976 to 1981, he served as a research associate at the Electronic Engineering Department of Tohoku University. During this period, he worked on biomedical transducers fabricated by micromachining. From 1981 to 1990 he was an associate professor. Since 1990 he has been a professor in the Department of Mechatronics and Precision Engineering, Tohoku University. His current research is an intelligent sensors and sensor–actuator systems fabricated by micromachining.